Ma, J. and Qi, X. and Zhao, Y. and Dong, Y. and Song, L. and Zhang, Q. and Yang, Y. 2016. Polyimide/mesoporous silica nanocomposites: Characterization of mechanical and thermal properties and tribochemistry in dry sliding condition. Materials and Design. 108: pp. 538-550.

Polyimide/mesoporous silica nanocomposites: Characterization of mechanical and thermal properties and tribochemistry in dry sliding condition

Jian Ma[1, 2], Xiaowen Qi[1, 2 *], Yuanliang Zhao[1, 2], Yu Dong[3], Laizhou Song[2, 4], Qinglong Zhang[1, 2], Yulin Yang[1, 2]

[1]School of Mechanical Engineering, Yanshan University, Qinhuangdao 066004, P. R. China

[2]Aviation Key Laboratory of Science and Technology on Generic Technology of Self-Lubricating Spherical Plain Bearing, Yanshan University, Qinhuangdao 066004, P. R. China

[3]Department of Mechanical Engineering; School of Civil and Mechanical Engineering, Curtin University, Perth, WA 6845, Australia

[4]College of Environmental and Chemical Engineering, Yanshan University, Qinhuangdao 066004, P. R. China

Abstract: Mesoporous silica (MPS) with tunable mesopore channels can be used to reinforce polymers and has great potential in tribological applications, which is rarely investigated by research community. In this study, comprehensive properties of polyimide (PI)/MPS composites were investigated. Specially, the tribochemistry of PI/MPS composites in dry sliding against bearing steel was explicitly studied by the combined use of X-ray photoelectron spectroscopy (XPS) and Raman analysis. The results demonstrated a slightly decreased tensile strength but increased modulus, microhardness and thermal stability of the PI/MPS composites. The incorporation of 1.5 wt.% MPS increased the anti-wear resistance of PI by more than 14-fold. This was highly associated with the formation of high-quality transfer film on the bearing steel counterpart surface. Relevant tribochemistry was thoroughly revealed by XPS analysis on the transfer film and Raman analysis on the worn surfaces. This study confirmed the high efficiency of using MPS to reinforce PI polymer for tribological applications and elaborated tribochemistry to further better understand tribochemical reactions in polymer-metal rubbing systems.

Keywords: Mesoporous materials, Polymer-matrix composites, X-ray photoelectron spectroscopy (XPS), Raman, Tribochemistry

1. Introduction

With the development of industries, the needs for high-performance friction materials continue to grow. For example, the global friction products market is estimated to grow at a compound average growth rate of 6.07% over the period 2014-2019, according to Technavio's report [1]. Such urgent need demands high-performance and low-cost friction materials. Polyimide (PI) is a versatile engineering plastic with its important application for non-lubrication friction, especially under harsh environment. Thus, excellent mechanical, thermal and tribological properties of PI-based composites are essentially needed to endure heavy load or elevated temperature. Mesoporous molecular sieves have attracted much attention since their first discovery [2-5]. Mesoporous materials benefit from two advantages including extremely high specific surface area (normally >500m^2/g) and interconnected mesoporous structures. The former provides reaction interfaces for mesoporous materials and others, whereas the latter facilitates the penetration of polymeric molecules into particulates in the formation of much stronger physical or chemical bonding, as evidenced in [6-9]. Mesoporous silica reinforced PI composites, typically PI film composites, are of interest among research community. Such PI-based films find multiple applications in areas for instance microelectrical industry [10] and selective separation [11]. However, the reinforcing effect of mesoporous on the mechanical and thermal properties of PI film is quite uncertain. For example, Cheng et. al synthesized PI/mesoporous silica nanocomposites with improved

*Corresponding author: Prof. Xiaowen Qi E-mail address: qxw_tougao@163.com

storage modulus, tensile strength and glass transition (T_g) [12]. Nevertheless, with the same PI matrix (ODPA-BAPP) but different kind of mesoporous silica, the modulus and tensile strength of PI/mesoporous silica composites prepared by Min decreased as the mesoporous silica content increases [13]. A similar case is also found in Lee's research, in which the tensile strength of PI/mesoporous silica composites monotonically declined as mesoporous silica content increases, while the tensile modulus varied in a rather irregular way [10]. Mesoporosity and interfacial bonding between the mesopore surface and PI molecules dominate the enhancing efficiency of mesoporous silica on properties of PI. In Min's study, the one SBA-15-1 mesoporous silica with larger pores is more efficient in enhancing the modulus of PI than that of SBA-15-2 [13]. Dissimilarly, inner surface treatment via coupling agent or chemical grafting aiming to promote the interfacial bonding does not always produce positive impact on the mechanical or thermal properties of PI matrix. The surface treatment of SBA-15 using ATS results in decreased tensile strength of PI [13], while on the contrary, tensile strength of PI reinforced with aminopropyl functionalized mesoporous silica is greatly enhanced [12]. The key of interfacial bonding affecting properties of PI matrix relies on whether the introduced chemical group on the mesopore surface could be well bonded with PI molecules or not.

Tribochemical process has been found in many rubbing systems under different rubbing conditions [14-17]. The intensity of tribochemical reactions could be provoked if chemically activated additives were added, such as the incorporation of CuS and PbS in polytetrafluoroethylene (PTFE) or nylon rubbing systems. The influence of tribochemical reactions on tribological properties of a rubbing system lies in the affected quality of transfer films. This is because the cohesion of transfer films and the adhesion between transfer films and mating surfaces could be strengthened by the formation of chemical bondings. Kapoor and Bahadur studied the transfer film bonding of nylon/CuS composites sliding against steel [14], in which CuS underwent the decomposition and reacted with oxygen and iron to form Fe_2O_3 and $FeSO_4$. Hence, the chemical bonding was increased between steel surfaces and transfer films, thus resulting in the decrease in the wear of transfer films and nylon composites. Another study showed that PTFE was decomposed in a rubbing process by generating activated F ion to react with metals in order to form metal fluorides [15]. In case of PI and PI composites, Li et al. found that the carbonation on the friction surface of a thermoplastic PI occurred in a dry sliding condition against steel [16]. At high temperature levels, Samyn and Schoukens found that the hydrolysis reaction between 120-180°C and imidisation of the bulk PI between 180-260°C took place and affected the lubrication effect of incorporated graphite flakes [17]. Samyn also studied the tribochemical behavior of PI by Raman spectroscopy and thermal analysis under different sliding temperatures [18-19] and high PV-conditions [20]. However, these studies mainly focused on the physicochemical changes of the bulk PI in friction but somehow less attention is paid in the tribochemistry between the PI matrix and the additives. One possible reason might be that PI has relatively high activation energy and cannot be easily activated to chemically react with other materials.

In the aspect of material tribology, research in the tribo-effect based on mesoporous materials was rarely seen. Romanes et.al introduced both as-synthesized and calcined Dallas amorphous material-1 (DAM-1) mesoporous silica (MPS) into epoxy matrix and studied their tribological properties [21]. The main concern of this research was microscratch behavior and surface and subsurface characteristics of epoxy composites reinforced with DAM-1. Their results revealed that DAM-1 tended to lower the friction of epoxy, and the mode of deformation as well as wear debris formation were altered by the formation of a reduced cross-linking density envelope around mesopores. This research established primarily an understanding on how MPS affected tribological behavior of polymer-matrix composites (PMCs). It also proved the high efficiency in using MPS for tribological applications. However, the influence of DAM-1 on the anti-wear property of epoxy was not involved in their research and relative wear mechanism still remains unrevealed. Further systematical investigations about MPS effects on tribological behavior of PMCs are of great interest. X-ray photoelectron spectroscopy (XPS) is a useful tool to analyze elements and chemical structure of chemical reaction products and is applied to reveal tribochemical process long ago [14-16]. The chemical bonding between polymer matrix and additives can be accurately detected by XPS analysis. But tribochemical process of PMCs sliding against steel is

more than chemical reactions between polymer matrix and additives. The physicochemical changes of the bulk polymer, such as re-orientation of the polymer molecular conformation at sliding surface, formation and/or decomposition of chemical group, are also equally critical on affecting the tribological properties of PMCs, which is beyond the ability of XPS analysis but is precisely the specialty of Raman spectrum analysis. Current study concentrates on the characterization of mechanical and thermal properties and tribochemistry of PI/MPS nanocomposites. Specially, the combined use of XPS and Raman analysis allows us to fulfill a meticulous investigation on the tribochemistry PI/MPS nanocomposites in dry sliding condition. Distinct differences were found in the tribochemistry of pure PI and PI/SMPS composites in dry sliding against steel. Rare tribochemical reactions between PI matrix and MPS were observed via XPS analysis while Raman analysis on the worn surfaces provided detailed information about the chemical structure changes of the PI.

2. Experimental details

2.1 Synthesis and surface modification of MPS

The synthesis of MPS was a modified route based on the previous work [22]. In a typical synthetic process, tetraethoxysilane (TEOS, 1 mol) and octylamine (OA, 0.674 mol) was mixed under stirring for 3-5 min. Then 50 mol deionized water with 0.45 mol hydrochloric acid solution was poured into the mixture prior to continuous stirring for additional 30 min. The white precipitate was collected after filtration and washed with ethyl alcohol to remove the residual reactant. After drying at 60°C for 6h, as-synthesized MPS was collected. The dried sample was calcined at 550°C for 6h to obtain final MPS with diameter of 170-200nm, as shown in Fig. 1. All chemicals were used without further purification. The specific surface area and pore diameter of calcined MPS measured by using N_2 absorption-desorption tests with Barrett–Joyner–Halenda (BJH) method were 826.9636 m^2/g and 3.5863nm, respectively. Fig. 2 demonstrates the N_2 adsorption–desorption isotherms of the calcined MPS with inserted curve of pore size distribution.

For the surface modification of MPS, a certain amount of MPS was ultrasonically dispersed in ethyl alcohol for 30min. Then silane coupling agent KH550 (Aladdin, $C_9H_{20}O_5Si$) was added with a mix ratio to MPS of 3ml:1g. After 4 h magnetic stirring, the MPS derivative was recovered by the filtration. MPS white powders were washed with deionized water and dried at 60°C. The surface modified MPS was thus abbreviated as SMPS.

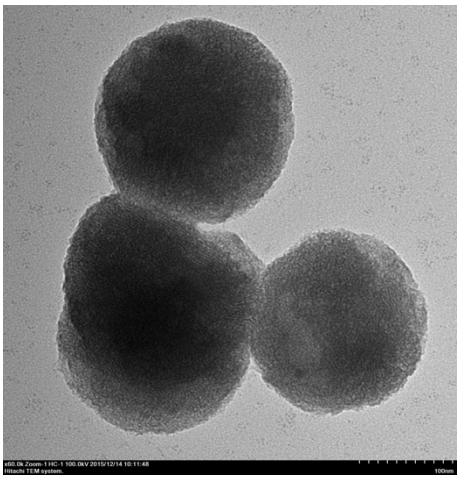

Fig. 1 TEM image calcined MPS

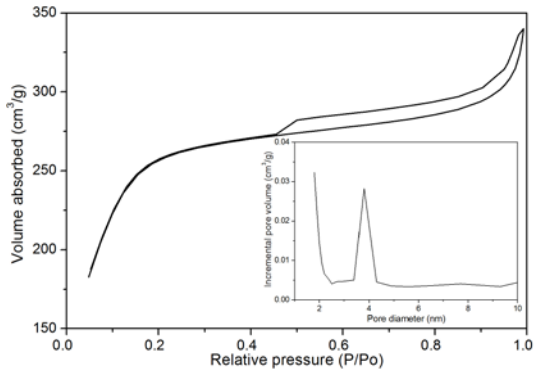

Fig. 2 N_2 adsorption–desorption isotherms of the calcined MPS

2.3 Preparation of PI and PI/SMPS composites

To synthesize PI, 4g 4,4′-diaminodiphenyl ether (ODA) were dissolved in 20ml dimethylacetamide (DMAC) with mechanical stirring at nitrogen atmosphere. 3,3′,4,4′-tetracarboxydiphthalic (ODPA) was added into the aforementioned mixture in three batches (2g, 2g, 2.23g). Each batch was washed with 8ml DMAC and completely dissolved via further stirring. Subsequently, DMAC was added to adjust the mixture viscosity. After the mixing reaction for about 4 h, polyamide acid (PAA) solution was finally obtained. Then triethylamine, acetic anhydride and methylbenzene were added to the PAA solution. After the further stirring for 1h, the solution was vacuum filtrated and the filter cake was washed 3 times using ethyl alcohol before being air dried at 90°C. The dried powder was ground and sieved to leave the fine part. After heating for 2h at 280°C, final PI powders were collected. SMPS and PI were mixed using a 3-D mechanical mixer and PI/SMPS composites were prepared with a molding technique of vacuum hot press with the molding pressure of 20MPa, heating temperature of 380°C and dwell time of 1h. The synthesized PI/SMPS composites were cut for different material analyses and testing.

2.4 Tribological tests

Tribological tests were conducted with an Anton Paar tribometer (for reciprocation tests) and a CSM tribometer (for rotation tests at a relatively high sliding speed), with the same ball-on-disk configuration. The reciprocating friction stroke was 8 mm and tests were conducted at normal loads of 5, 10 and 15 N, respectively. Average sliding speeds were 0.04, 0.06 and 0.08m/s and the sliding distance was fixed at 250m. The rotation tests were carried out at a normal load of 10N and linear sliding speeds of 0.15, 0.2, 0.25, 0.3 and 0.35m/s. The sliding distance was 500m. The tests were performed in ambient air environment at room temperature. The COF curves can be recorded by both testers and average COF values at the steady sliding stage were calculated accordingly. The wear tracks of the worn PI and PI/SMPS composites were measured with an Anton Paar Indepention using an optical microscope with 3-D scanning functions. Optical images for wear tracks and corresponding 3-D scanning images observed from the cross-sectional area of wear tracks at random positions were directly acquired with the aid of Image Plus software. GCr15 bearing steel ball with the diameter of 6 mm was commercially purchased. Both the steel ball and PI/SMPS composites were ultrasonically cleaned using acetone for 10 min and further absolute alcohol for 15 min prior to tribological tests. At least 10 different positions along the sliding direction within 3-D scanning images for wear tracks were selected to measure the cross-sectional area. The wear volume $\triangle V(\mu m^3)$ was then calculated by Equation (1):

$$\Delta V = Sd \tag{1}$$

Where d is the length or the sliding perimeter (mm) during the rotation test and S is the cross-sectional area of wear track). The specific wear rate can be calculated by Equation (2):

$$k = \frac{\Delta V}{FL} \tag{2}$$

Where F is the applied load (N) and L is the sliding distance (m). Each test was repeated at least three times for data reproducibility and average values and standard deviations were reported accordingly.

2.5 Characterization

Tensile tests were performed according to ISO 527-1: 1993 standard. Thermogravimetry (TGA, NETZSCH) measurements were performed at Ar atmosphere from 50°C to 900°C at heating rate of 10°C/min. The wear tracks and transfer films of PI/SMPS composites were examined using Anton Paar Indepention to obtain optical images and 3-D scanning images. A Hitachi S-4800 Field emission scanning electron microscope (FESEM) was used to examine fractured and worn surfaces of PI/SMPS composites. XPS spectrum was determined using a PHI-5400 system (Perkin Elmer, U.S.A) with monochromated AlKa and a charge neutralizer. The pass energies of wide-angle and small-angle scanning were 120 and 50 eV, respectively. The C1s binding energy was set to be 285 eV for the calibration purpose.

Raman tests on pristine PI surface and worn surfaces of pure PI and 1.5 wt.% PI/SMPS composite were performed on Renishaw RM2000 with applied laser wavelength of 532nm at a resolution of $1cm^{-1}$.

3. Results and discussion

3.1 Mechanical property and thermal stability

Typical stress/strain curves of PI/SMPS composites are shown in Fig. 3 and the average tensile properties including tensile stress at break σ_B, tensile strain at break ε_B, tensile stress at yield σ_y, tensile strain at yield ε_y, tensile strength σ_M and modulus E are summarized in Table 1. Modulus of PI/SMPS composites was increased except for that of the one with 0.5 wt.% SMPS loading. The modulus of 1.5 wt.% PI/SMPS composite was about 38.8% greater than that of the pure PI. However, tensile strength of PI/SMPS composites was moderately decreased and the strain at break was greatly decreased in comparison with those of pure PI. This means that the PI/SMPS composites became more fragile than pure PI. The decreased tensile strength of the PI/SMPS composites is due to that the interfacial strength between SMPS and PI molecules is less comparable to that between PI molecules [12] and that the relatively small pore space of SMPS absorbs less energy than that in pure PI before tensile failure [23]. Another important factor might be the particle aggregation of the SMPS within the PI matrix, as roughly indicated in the circled area in the microstructure of fractured surfaces of PI/SMPS composites shown in Figs. 4d-f. These aggregated SMPS particles acted as fracture initiation when tensile load was applied and thus produced negative effect on the tensile property of PI/SMPS composites. Contrastively, particle aggregation was less obvious in cases of 0.5 and 1 wt.% PI/SMPS composites (Figs. 4b and c). But some small voids and scattered particles that resulted from debonding of tiny particle aggregation from the PI matrix were still observed if inspected carefully. This is another indicator that why these two composites showed decreased tensile strength.

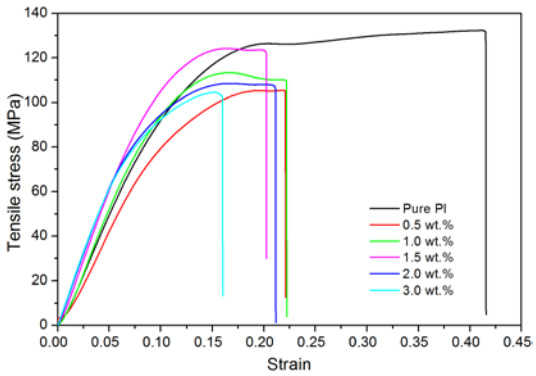

Fig. 3 Typical stress/strain curves of PI/SMPS composites

Table 1 Tensile properties of PI/SMPS composites*

SMPS loading (wt.%)	σ_B (MPa)	ε_B	σ_y (MPa)	ε_y	σ_M (MPa)	E (MPa)[a]
0	132.29	0.415	126.35	0.2	132.29	941.76
0.5	105.28	0.244	104.94	0.191	105.28	845
1.0	109.95	0.223	113.23	0.172	113.23	1070.47
1.5	122.83	0.203	124.14	0.166	124.14	1306.5
2.0	106.04	0.215	108.42	0.171	108.42	1293.12
3.0	103	0.159	--	--	108.05	1284.66

* Standard deviations of all experimental values are less than 6%.

[a] Curve fittings from strain range of 0.5-1.0%.

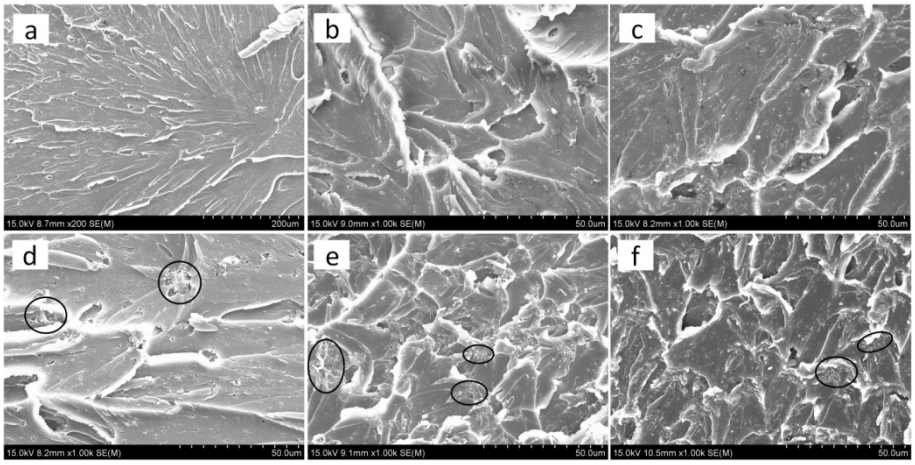

Fig. 4 FESEM images of fractured surface of PI composites with SMPS content of a) 0 wt.%, b) 0.5 wt.%, c) 1 wt.%, d) 1.5 wt.%, e) 2 wt.% and f) 3 wt.%.

Typical nanoindentation curves of PI reinforced with different loadings of SMPS are shown in Fig. 5. The indentation depths of the PI/SMPS composites specimen were smaller than that of the pure PI, indicating an increased microhardness of the PI/SMPS composites. More specifically, the nanoindentation properties are listed in Table 2. All the nanoindentation properties of PI/SMPS composites were promoted except for the EIT and E* of the 1 wt.% PI/SMPS composite. Such results are predictable because the incorporation of inorganic fillers usually promotes the hardness of polymer matrixes [24].

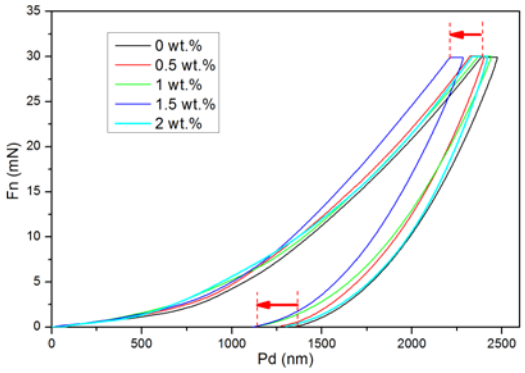

Fig. 5 Nanoindentation curves of neat PI and PI/SMPS composites

Table 2 Nanoindentation properties of PI/SMPS composites

SMPS loading (wt.%)	Nanoindentation properties			
	[1]HIT (O&P) [MPa]	[2]HVIT (O&P) [Vickers]	[3]EIT (O&P) [GPa]	[4]E* (O&P) [GPa]
0	265.120±1.768	24.533±0.164	4.033±0.075	4.432±0.083
0.5	309.550±7.726	28.668±1.042	4.500±0.047	4.945±0.052
1.0	328.326±12.154	30.407±1.126	3.892±0.080	4.277±0.088
1.5	359.905±7.620	33.331±1.258	4.440±0.289	4.879±0.318
2.0	310.607±5.691	28.766±1.361	4.475±0.330	4.917±0.362

[1]Indentation hardness, [2]Vickers hardness, [3]Indentation modulus, [4]Plane strain modulus

TGA curves of the pure PI and PI/SMPS composites are shown in Fig.6. It can be seen that the thermal stability of the PI/SMPS composites were enhanced in comparison to the pure PI, as indicated with the dotted line. The pure PI lost 5 % of its weight at 515°C whereas for the PI/SMPS composites the temperature at 5 % weight loss progressively increased from 535°C to 542°C as the SMPS loading varied from 0.5 wt.% to 3 wt.%. Despite with very low SMPS loadings, the degradation temperature of the PI was increased by nearly 27°C. This suggested that the PI chains were successfully penetrated in the mesopore network of the SMPS, since the degradation of the PI matrix starts from the outer surface inward and thus promotes the degradation temperature [25].

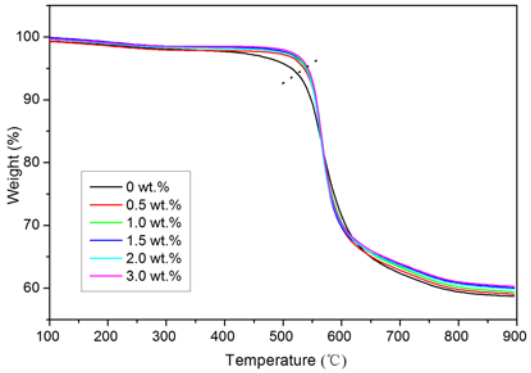

Fig. 6 TGA thermograms of pure PI and PI/SMPS composites

3.2 Tribological behavior

3.2.1 COF and specific wear rate

The COF and specific wear rate variations of PI/SMPS composites as a function of SMPS content at 10N with a reciprocation sliding speed of 0.04 m/s are shown in Fig. 4. The COF of PI/SMPS composites gradually decreased as the SMPS content increased up to 1.5 wt.%. Then the COF increased with a further increase in the SMPS content. Specific wear rate of PI/SMPS composites decreased abruptly with the addition of SMPS when compared with that of pure PI. A further decrease occurred up to the SMPS content of 1.5 wt.%, indicating excellent reinforcing effect of SMPS on the wear resistance of PI. Hence, the optimum SMPS content was detected at 1.5 wt.% in order to achieve better frictional reduction and anti-wear properties of PI/SMPS composites. Both COF and specific wear rate of PI were greatly decreased with the incorporation of SMPS into PI matrix. More specifically, COF and specific wear rate of PI composites reinforced with 1.5 wt.% SMPS reached much lower values of 0.242 and $0.48\times10^{-15}m^3N^{-1}m^{-1}$, with the reductions of over 27 and 93%, as opposed to those of pure PI at 0.333 and $6.96\times10^{-15}m^3N^{-1}m^{-1}$, respectively. The significant improvement in tribological properties of PI/SMPS composites might be associated with their promoted modulus and micro-hardness (Figs. 3, 5) which are believed to be effective in improving the anti-adhesion ability of polymeric composites and suppressing the generation of wear debris [26]. The generation of high-quality transfer films owing to the interfacial chemical reaction is another crucial factor that affects the tribological properties of the PI/SMPS composites, which was explained elaborately in subsequent sections. It is also noticed that the enhancement efficiency on the wear resistance of PI using SMPS is comparable to that based on modified graphene (93% vs. 95%increases [26]). However, much more increment in the friction-reduction (SMPS vs. modified graphene: 27% vs. 12%) becomes manifested. Considering the facile synthetic method and the cost, the use of SMPS as reinforcing additives for improving tribological properties of PMCs could be regarded as a cost-effectiveness and practically effective approach.

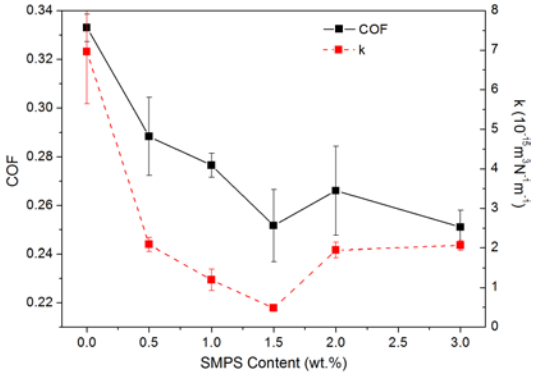

Fig. 7 COF and specific wear rate of PI/SMPS composites as a function of SMPS content at 10N and 0.04 m/s for reciprocation sliding.

The 1.5 wt.% PI/SMPS composite was chosen to further investigate the effects of applied load and sliding speed on its friction and wear properties. Fig. 5 shows the COF and specific wear rate of PI composites reinforced with 1.5 wt.% SMPS at different reciprocation sliding speeds as a function of applied load. The applied load significantly affected the COF of composites. However, the COF was barely changed at the same applied load when the reciprocation sliding speed varies. The COF was found to be proportional to the applied load at all reciprocation sliding speeds. This is most likely to be associated with the plastic deformation of asperities in contact [27]. For the specific wear rate at all reciprocation sliding speeds, it underwent less noticeable changes at applied loads of 5 and 10 N, but significant increases at 15 N. In particular, at 0.04 and 0.08 m/s, specific wear rate moderately increased, whereas it decreased at 0.06 m/s when the applied load was increased from 5 to 10 N. Fig. 6 shows the correlations of COF and specific wear rate of PI composites reinforced with 1.5 wt.% SMPS with different sliding speeds at the applied load of 10N. The COF was relatively high at sliding speed of 0.15 m/s. But as the sliding speed exceeded 0.2 m/s, the COF was maintained at a relatively low level, fluctuating between 0.2075-0.2225 when varying the sliding speed from0.2-0.35 m/s. The specific wear rate increased as the sliding speed increased up to 0.25 m/s, and then decreased with its further increase. The friction and wear of such composites appeared to be affected by the sliding speed at the constant applied load.

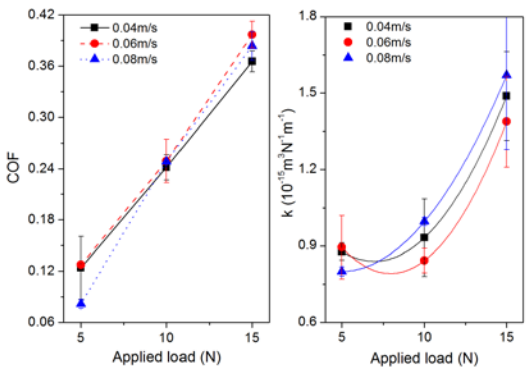

Fig. 8 COF and specific wear rate of PI composite reinforced with 1.5 wt.% SMPS as a function of applied load at different reciprocation sliding speeds of 0.04, 0.06 and 0.08 m/s.

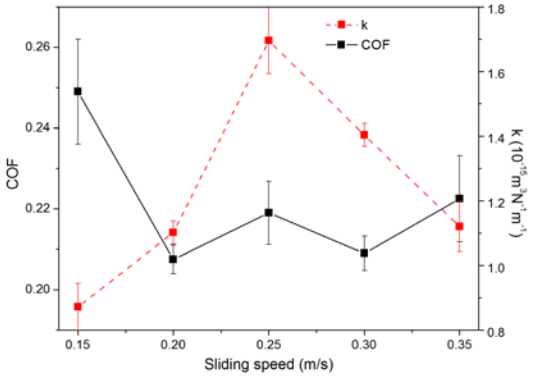

Fig. 9 COF and specific wear rate of PI composites reinforced with 1.5 wt.% SMPS as a function of sliding speed at the applied load of 10N.

3.2.2 Wear morphology

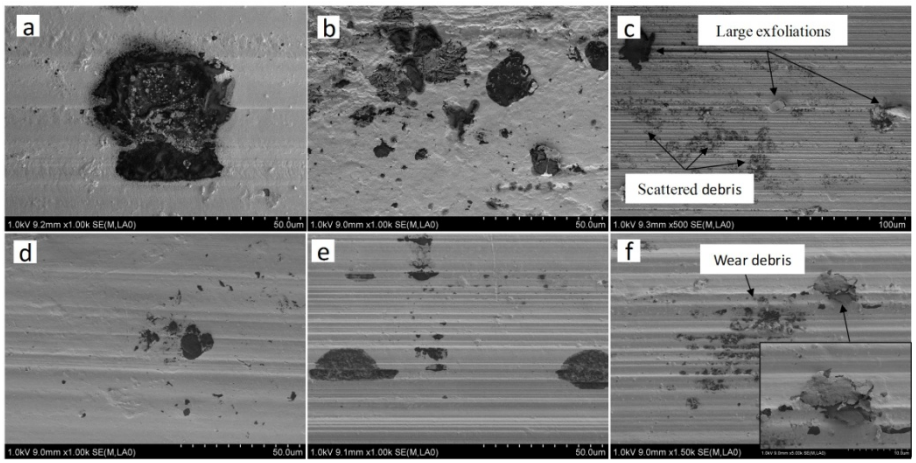

Fig. 10 FESEM micrographs of worn surfaces of PI composites with different SMPS contents: a) 0 wt.%, b) 0.5wt.%, c) 1wt.%, d) 1.5wt.%, e) 2wt.% and f) 3 wt.%

FESEM micrographs of worn surfaces of PI composites at different SMPS contents from 0 to 3 wt.% are presented in Fig. 8. As illustrated in Fig. 8a, worn surfaces of pure PI appeared to be relatively flat with peeled large and thin slices attached to worn surfaces. Wrinkles due to plastic deformation were manifested along the sliding direction and plenty of small worn debris was scattered on worn surfaces as well. The wear mechanism of pure PI sliding against GCr15 steel was ascribed to the delamination and plastic deformation .Fig. 8b shows the worn surface of PI composites reinforced with 0.5 wt.% SMPS. The wear debris clearly became smaller in comparison to that in Fig. 8a and plastic deformation was also observed. The wear of lower regions was relatively mild with few wear debris, which might be caused by the uneven SMPS dispersion within PI matrix. A cluster of narrow grooves was evident on the worn surface of PI composites reinforced with 1 wt.% SMPS, Fig. 8c. Large exfoliation and scattered wear debris were also found on the wear surface, indicating that the main wear mechanism is delamination and abrasive wear. However, plastic deformation was not observed at all. This phenomenon suggested that the load capacity of PI composites reinforced with 1 wt.% SMPS might be improved, which contributes to the anti-wear property of composites. Fig. 8d corresponds to the worn surface of PI composite reinforced with 1.5 wt.% SMPS. The worn surface was relatively smooth, with a few wear debris and shallow grooves. It was indicated that the generation of wear debris and exfoliation was suppressed. This wear characteristic is related to its low specific wear rate. As the SMPS content increased to 2 wt.%, demonstrated in Fig. 8e, the grooves were getting dense again with more observed exfoliation and wear debris, resulting in a decreased anti-wear property. When the SMPS content was increased up to 3 wt.% (Fig. 8f), the wear was much more severe, and the composite surface was even more crushed, as depicted in the inserted magnified micrograph in Fig. 8f. Such morphology might be induced by the micro plough effect of the particle aggregation evidenced in Figs. 4e and f.

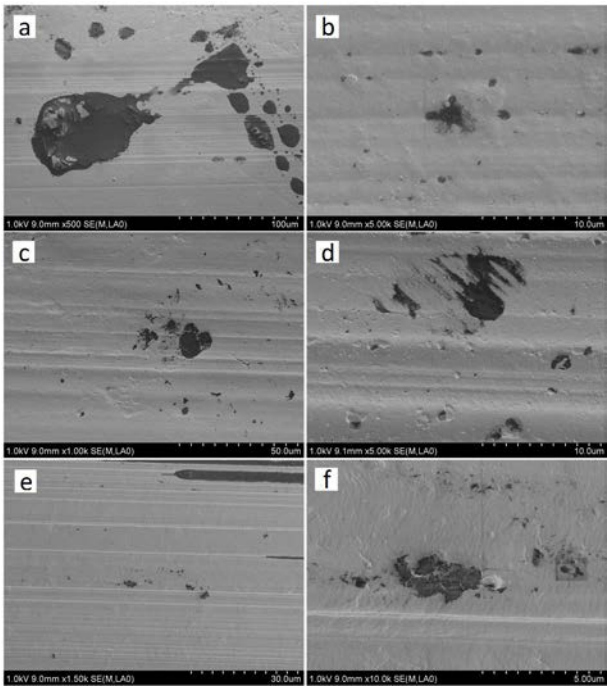

Fig. 11 Low and high-magnification FESEM micrographs of the worn surface of PI composites reinforced with 1.5 wt.% SMPS at different applied loads: a) and b): 5N, c) and d): 10N and e) and f): 15N

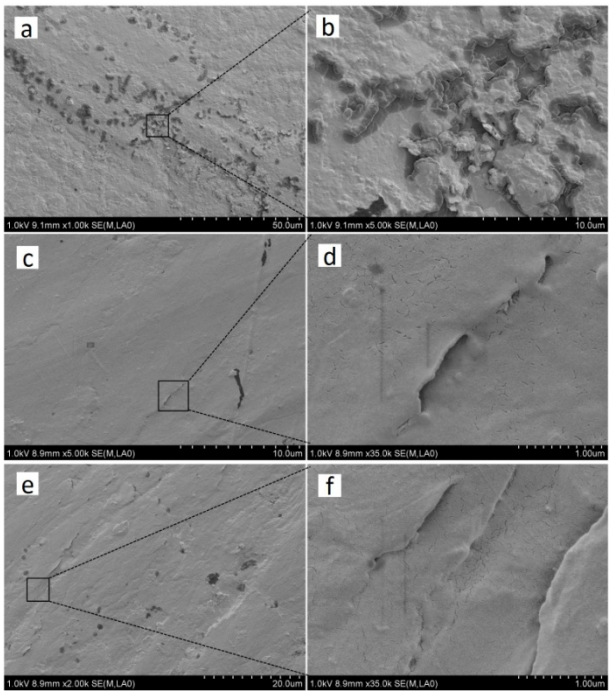

Fig. 12 Low and high-magnification FESEM micrographs of the worn surface of 1.5 wt.% PI-SMPS composite at different sliding speeds: a) and b): 0.15m/s, c) and d): 0.25m/s, and e) and f): 0.35m/s.

Low and high-magnification FESEM micrographs from the worn surface of PI composites reinforced with 1.5 wt.% SMPS at different applied loads are shown in Fig. 9. The worn surface of such composites at 5N was relatively flat with few large exfoliations and shallow grooves, Fig. 9a. Small wear debris was rarely found even at a high-magnification micrograph depicted in Fig. 9b. As the applied load increased to 10N, the exfoliation became less noticeable but the grooves were more apparent (Fig. 9c). Plenty of wear debris was observed in the magnified micrograph shown in Fig. 9d, signified by the promoted severity of wear. Fig. 9e shows the worn surface of composites at 15N, which clearly reveals that the exfoliation was greatly decreased but the grooves became wider and deeper. The magnified micrograph of the worn surface presented wrinkles under plastic deformation, but wear debris was barely found. As the applied load increased from 5 to 15N, the wear mechanism appeared to transform from exfoliation to abrasive wear and plastic deformation.

FESEM micrographs of the worn surface of PI composites reinforced with 1.5 wt.% SMPS at different sliding speeds are shown in Fig. 10. At 0.15 m/s, the wear was characterized by delamination whose region was mainly in the central area of wear tracks. The magnified micrograph in Fig. 10b corresponding to the quadrate area in Fig. 10a showed the structural details of wear fragments. As the sliding speed increased to 0.25 m/s, the worn surface was smooth with few wear debris. But the initiation of micro-cracks occurred, illustrated in the magnified micrograph in Fig. 10d. Fig. 10e shows the worn surface at 0.35 m/s in which wear debris, micro-cracks and shallow wear grooves were observed. In the magnified micrograph of Fig. 10f, the initiation of micro-cracks expanded when compared with those in Fig. 10d.

3.2.3 Transfer film

Transfer film generated on the mating surface plays an important role in controlling friction and wear in dry sliding of polymer-metal rubbing systems. Its uniformity is critical to control the wear, whereas the physical state of transfer films dominates the frictional coefficient [28, 29]. Fig. 11 shows optical images of transfer films on the GCr15 steel ball

surface sliding against pure PI and PI/SMPS composites. Transfer film shown in Fig. 11a corresponding to pure PI was non-uniform and discontinuous. It was torn apart with ribbon-like pieces left along the sliding direction. Besides, the wear scar of the steel ball was so big that its diameter was nearly 1mm, resulting in severe wear for both the steel ball and pure PI. Comparatively, transfer films of PI/SMPS composites seen in Figs. 11b-f were more uniform and much thinner regardless of the SMPS content. Meanwhile, the wear of the steel ball was also significantly reduced based on the dimension of wear scar. Fig. 12 demonstrates 3-D scanning images of transfer films for pure PI and PI composites reinforced with 1.5 wt.% SMPS. As seen from Fig. 12a, the transfer film of pure PI was thick and non-uniform with a clearly visible edge, as opposed to thin and uniform transfer film of PI composites reinforced with 1.5 wt.% SMPS, Fig. 12b. It seems to be hard to tell the transfer film of such composites from the steel substrate. Accordingly, the incorporation of SMPS into PI matrix is believed to promote the quality of transfer films. It is meaningful to investigate why the transfer films generated by the PI and PI/SMPS composites considerably varied. One critical fact that affects the quality of transfer film is tribochemistry in rubbing process [], which was elaborately investigated in the next section.

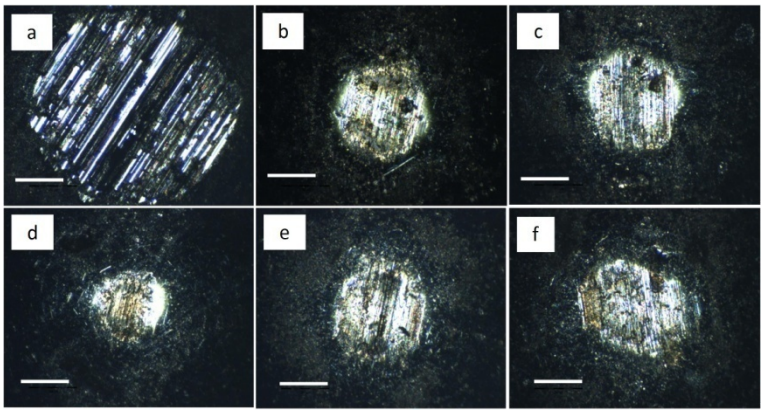

Fig. 13 Optical images of transfer films on steel balls at different SMPS contents: a) 0 wt.%, b) 0.5 wt.%, c) 1 wt.%, d) 1.5 wt.%, e) 2 wt.% and f) 3 wt.% in reciprocation tests at 10 N and 0.04 m/s. Scale bars represent 200μm.

Another notable phenomenon lies in the different COF curves of pure PI and PI/SMPS composites shown in Fig. 13. The COF curve of pure PI presents an evident, long-time and fluctuant transition from the running-in to the steady periods. In contrast, the COF transition of PI/SMPS composites has been hardly detected. Considering the dominant effect of the physical state of the transfer film on the COF of PMCs, it is deduced that the transfer film may have been formed within the running-in period. The formation of transfer film was apparently accelerated with the addition of SMPS into PI matrix.

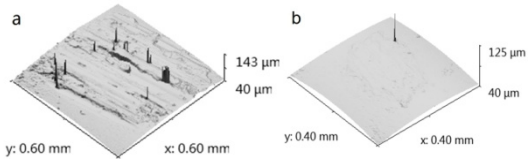

Fig.14 3-D scanning images of transfer films: a) pure PI and b) PI composites reinforced with 1.5 wt.% SMPS.

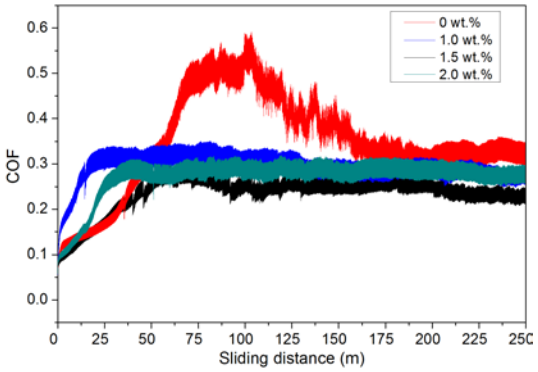

Fig.15 COF curves of pure PI and PI/SMPS composites in reciprocation tests at10N and 0.04 m/s.

3.2.4 Tribochemistry

XPS and Raman analysis were employed to understand the tribochemistry in the rubbing process and how the tribochemistry affects the tribological properties of PI/SMPS composites. Survey spectra of XPS results were given in Fig. 14 along with their relative atomic concentrations summarized in Table 1. Relative atomic concentrations of C element in PI composites reinforced with 1.5 wt.% SMPS, transfer films of pure PI and corresponding composites became sequentially decreased while those of O and N elements increased accordingly. The increased atomic concentration for O element was attributed to air and water vapor under ambient atmosphere by reacting with Fe element from the steel substrate. For the PI/SMPS composites the increased atomic concentration of O might be also caused by the reaction of released C from the cleavage of C=C bond with oxygen (see Raman analysis). However, the N_2 at the ambient atmosphere is too chemically inert to participate in the tribochemical reaction. Hence, it is presumed that the N from the PI reacted with other radicals or functional groups to form new substances that remained within the transfer film and caused the increase of the N concentration. This means that PI molecules underwent decomposition during the rubbing process. The Fe element in transfer films for both pure PI and PI composites reinforced with 1.5 wt.% SMPS at etching time of 20s showed three valence states, namely bivalent iron, trivalent iron, and elemental iron. Compared with the transfer film of pure PI, the relative atomic concentration of Fe element in the transfer film of PI composites reinforced with 1.5 wt.% SMPS decreased. Nevertheless, it was not the case for the relative atomic concentration of Si within such composites and their transfer film. Besides, survey spectra of the transfer film for PI composites reinforced with 1.5 wt.% SMPS at the etching time of 0 and 20s made significant differences. At the etching time of 0s, the Fe element was hardly detected and the intensity of Si element appeared to be much stronger. It is worth mentioning that the etching depth was about 5.6nm with etching time of 20s. This implied that on one hand, the transfer film was well established and pre-deposited on the steel surface, most likely in running-in period. The wear at this state was mainly caused by the replacement of transfer film by subsequent passes, which was considerably slow and often resulted in a very low wear rate [29]. On the other hand, it was suggested that the transfer film was physically stable and the adhesion between the transfer film and steel substrate was so strong that the transfer film could survive from successive passes. This characteristic of the transfer film is essentially important to improve the wear resistance of PI/SMPS composites.

Fig. S1 shows XPS spectra of C1s for PI composites reinforced with 1.5 wt.% SMPS and the transfer films of pure PI and corresponding PI/SMPS composite. All three spectra presented one prominent peak and two shifted signals. However, prominent peaks of transfer films for both pure PI and PI composites reinforced with 1.5 wt.% SMPS at 284.8 eV were slightly shifted compared with that of PI composites reinforced with 1.5 wt.% SMPS at 385eV. The same applied to the other two shifted signals. The relative atomic concentration of each functional group, as shown in Table S1, was also differentiated. This mainly arose from the carbonization induced by the frictional heat, as proposed by Li et al. [16], which suggested that PI matrix were involved with tribochemical reactions.

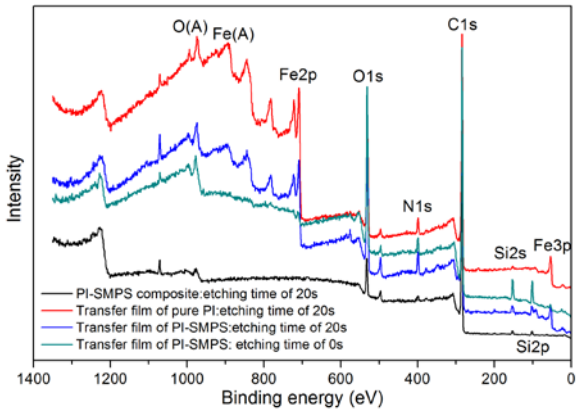

Fig. 16 Survey spectra of PI composites reinforced with 1.5 wt% SMPS and corresponding transfer films with a sliding condition at 10N and 0.15m/s.

Table 3 The relative atomic concentration of PI composites reinforced with 1.5 wt.% SMPS and transfer films of pure PI and corresponding PI/SMPS composites

Elements	Relative atomic concentration (At.%)		
	PI composites reinforced with 1.5 wt.% SMPS	Transfer film of pure PI	Transfer film of PI composites reinforced with 1.5 wt.% SMPS
C1s	81.94	72.04	64.42
O1s	9.34	14.22	18.35
Fe2p	--	9.36	5.77
N1s	2.95	3.31	4.49
Na1s*	1.84	1.07	2.09
Cr2p	--	--	0.95
Si2p	3.26	--	3.19
Cl2p*	0.68	--	0.73

*Note that contaminants such as NaCl may be incorporated during XPS tests or tribological tests.

XPS spectra of Fe2p, O1s, N1s and Si2p for transfer films of pure PI and PI composites reinforced with 1.5 wt% SMPS are summarized in Fig. 16. The Fe2p spectrum showed two prominent peaks at 709.8 and 706.8eV, corresponding to Fe_2O_3 and elemental iron, respectively. This indicated that the Fe element from the steel ball reacted with O_2 or H_2O or both in the atmosphere with or without SMPS. However, the intensity and the peak area of the Fe2p spectrum for the transfer film of pure PI were higher than those of PI composite counterpart reinforced with 1.5 wt.% SMPS. This was also observed from the relative atomic concentration of the Fe2p in Table 1. The possible reason can be due to relative low coverage of transfer film for pure PI with the exposure of a part of worn steel ball, Fig. 7a. Consequently, not only Fe element in the transfer film of PI composites reinforced with 1.5 wt.% SMPS but also the worn steel ball were detected in XPS analysis. Nonetheless, owing to the high coverage of transfer film, Fe element was mainly detected from the transfer film of PI composites reinforced with 1.5 wt.% SMPS. The peak at 532.5eV in O1s spectrum was indicative of the presence of C=O binding and the silica. On the other hand, the peak at 530eV represented Fe_2O_3, as formerly confirmed in the Fe2p spectrum. Diverse N1s spectra were detected for the transfer films of pure PI and PI composites reinforced with 1.5 wt.% SMPS. A prominent peak at 399.7 eV existed in both spectra, representing the C-N binding illustrated in Fig. 3. The extra peak at 398.6 eV in the spectrum of transfer films for PI composites reinforced with 1.5 wt.% SMPS suggested the occurrence of Si-N binding due to the chemical reaction taking place between SMPS and PI molecules. Both Si2p spectra of PI composites reinforced with 1.5 wt.% SMPS and their transfer films demonstrated the presence of silica based on a prominent peak at 102.5 eV. The peak at 101.7 eV in the Si2p spectrum of the transfer film for such PI composites represented the Si-N binding, in good accordance with the peak at 398.6 eV in the N1s spectrum. This means that PI underwent decomposition and reacted with silica in the rubbing process. This is rather remarkable because the activation energy of PI is relatively high at nearly 25kcal/mol, as opposed to 7kcal/mol for PTFE. Silica is also relatively chemically stable. For the first time, it was reported that tribochemical reactions between PI polymeric molecules and SMPS additives could strengthen our understanding on the threshold of tribochemical reactions in polymer-metal rubbing systems, which means that tribochemical reactions take place even for polymer matrix with high activation energy in particular conditions.

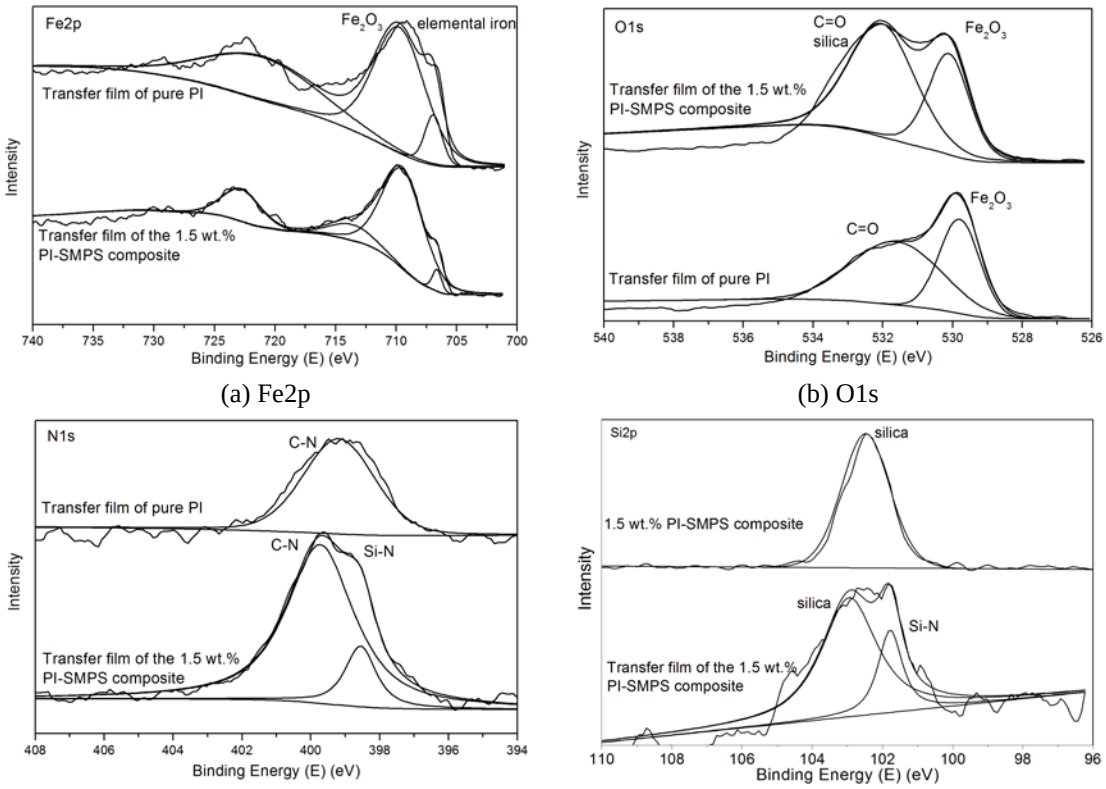

Fig. 17 XPS spectra of transfer films for pure PI and PI composites reinforced with 1.5 wt.% SMPS : (a) Fe2p, (b) O1s, (c) N1s and (d) Si2p.

Raman spectrum of different worn surfaces was shown in Fig. 18. The characteristic absorption bands of PI, including at 1780 and 1720 cm^{-1} (asymmetric and symmetric C=O stretching vibrations, imide Ⅰ), 1600 and 1460 cm^{-1} (aromatic C=C stretch), 1368 cm^{-1} (C-N-C axial vibration, imide Ⅱ), 1236 cm^{-1} (C-O stretch) and 1092 cm^{-1} (C-N-C transverse vibration, imide Ⅲ) were observed in Raman spectrum of unworn and worn PI, indicating no chemical degradation for the pure PI. However, relative intensities of several characteristic Raman bands of the worn and unworn surface of pure PI are obviously varied, as shown in Fig. 19. In Samyn's study [18, 19], it is demonstrated that the variation in relative intensity of these bands reflects their re-orientation relative to the phenyl ring in the imide structure, which is related to the friction and wear of PI. In the case of PI/SMPS composite, significant differences were observed in the Raman spectrum of its worn surface. The bands of imide Ⅱ and aromatic C=C stretch were absent. This implies the cleavage of the C-N and C=C bonds and the decomposition of PI molecules in friction, which released empty orbit of the element N. Thus tribochemical reaction between the decomposed PI molecules and the MPS occurred as evidenced by the detection of Si-N chemical bond in the XPS analysis. The cleavage of C-N bond is predictable because of the detection of Si-N bond in XPS analysis. What is surprising is that the cleavage of aromatic C=C bond whose typical cleavage condition is in pyrolysis at 500-600°C [30]. In friction, flash temperature at micro contact area of the two rubbing materials can reach as high as 1100°C within few ms [31]. Such elevated flash temperature might be responsible for the cleavage of C=C bond. The released C reacted with oxygen in atmosphere and increased the atomic concentration of O, as shown in Table 3. The incorporation of MPS into PI matrix resulting in the penetration of PI molecules into the mesoporous network of the MPS might be the key that the tribochemical changes take place in rubbing process. Comparably, tribochemical change is limited in re-orientation of the surface molecules in the case of pure PI.

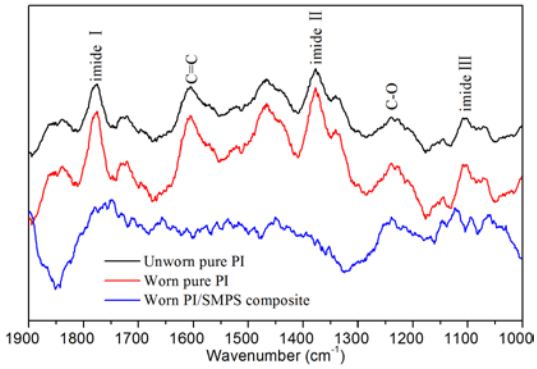

Fig. 18 Raman spectrum of different worn surfaces

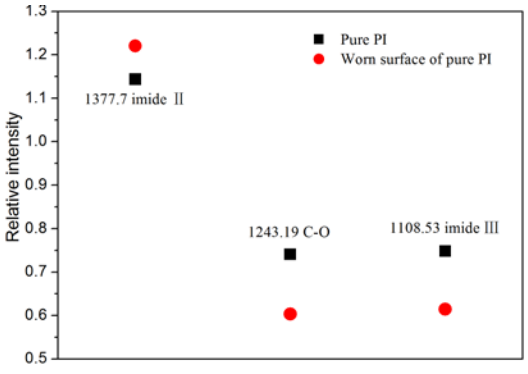

Fig. 19 Relative intensities of characteristic Raman bands, inserted numbers refer to the wavenumbers in Fig. 18

The eventual outcome of friction is the wear and/or failure of the friction material. The material removal, more referred as 'wear mechanism', is paramount in controlling the friction and wear of a friction material. Tribochemistry of the PI/SMPS composites in dry sliding against bearing steel influences the tribological properties of the friction pair via altering the wear mechanism. For pure PI in friction, the bulk material is removed mainly in two ways: the first removal by the counterpart surface asperities and the second removal from the transfer film on the counterpart surface. The first removal obviously causes high wear rate, while the second removal is rather moderate. But the adhesion between the transfer film and the steel substrate of the pure PI is very weak due to the weak bonding such as Van der Waals force. Thus the second removal for the pure PI also remains in high level, as reflected in Fig. 4. Nevertheless, significant changes in the wear In the case of the PI/SMPS composites, the first removal only occurs in the very short running-in period. During steady wear, in which the transfer film already well formed, the second removal is the dominant wear mechanism. Different with pure PI, the cohesion of the transfer film and the adhesion between the transfer film and the steel substrate of the PI/SMPS composites are strongly enhanced by the chemical bondings. Thus the wear is mainly caused by the replacement of transfer film by subsequent passes, as also demonstrated in the XPS analysis. In such way, the friction and wear behavior of PI/SMPS composites in dry sliding against bearing steel is affected and their tribological properties are significantly enhanced.

4. Conclusions

Based on the results obtained in this study, the following conclusions can be drawn:

1) Modulus, microhardness and thermal stability of PI/SMPS composites were increased whereas the tensile strength was slightly decreased.
2) Incorporation of SMPS greatly promoted the tribological properties of PI, which relied on several aspects: (1) the generation of wear debris and large exfoliation were restrained; (2) the load capacity of PI/SMPS composites was promoted and (3) the quality of transfer films was improved.
3) Tribochemistry involved in the dry sliding of PI/SMPS composites against bearing steel was thoroughly revealed by the combining use of XPS and Raman analysis. For the pure PI, the main tribochemical change was the re-orientation of surface molecules in friction. In the case of PI/SMPS composites, the tribochemical process included the decomposition of surface PI molecules and the subsequent reaction between the decomposed PI molecules and the activated SMPS. Such tribochemical changes greatly improved the quality of transfer film, which enhanced the tribological properties by altering the wear mechanism from direct peeling for the pure PI to the replacement of transfer film in friction for the PI/SMPS composites.

5. References

[1] http://www.fastmr.com/prod/1036229_global_friction_products.aspx

[2] Kresge CT, Lenowicz ME, Roth WJ, Vartuli C, Beck JS. Orderedmesoporous molecular sieves synthesized by a liquid-crystal templatemechanism. Nature 1992;359: 710-712.

[3] Shang L, Bian T, Zhang B, Zhang D, Wu LZ, Tung CH, Yin YD, Zhang T. Graphene-supported ultrafine metal nanoparticles encapsulated by mesoporous silica: robust catalysts for oxidation and reduction reactions. Angew Chem Int Edit 2014;53: 250-254.

[4] van Rijt SH, Bölükbas DA, Argyo C, Datz S, Lindner M, Eickelberg O. Protease-mediated release of chemotherapeutics from mesoporous silica nanoparticles to ex vivo human and mouse lung tumors. Acs Nano 2015;9: 2377-89.

[5] Li L, Sun Y, Cao B, Song H, Xiao Q, Yi W. Preparation and performance of polyurethane/mesoporous silica composites for coated urea. Mater Design 2016;99: 21-25.

[6] Murakami K, Yu X, Watanabe S, Kato T, Inoue Y, Sugawara K. Synthesis of thermosensitive polymer/mesoporous silica composite and its temperature dependence of anion exchange property. J Colloid Interf Sci 2011;354: 771-776.

[7] Kudasheva A, Sorribas S, Zornoza B, Téllez C, Coronas J. Pervaporation of water/ethanol mixtures through polyimide based mixed matrix membranes containing ZIF-8, ordered mesoporous silica and ZIF-8-silica core-shell spheres. J Chem Technol Biot 2015;90: 669-677.

[8] Inagaki S, Guan S, Ohsuna T, Terasaki O. An ordered mesoporous organic-silica hybrid material with a crystal-like wall structure. Nature 2002;416: 304-307.

[9] Ye X, Wang J, Xu Y, Niu L, Fan Z, Gong P, et. al.. Mechanical properties and thermostability of polyimide/mesoporous silica nanocomposite via effectively using the pores. J Appl Polym Sci 2014;131: 205-212.

[10] Lee T, Park SS, Jung Y, Han S, Han D, Kim I, Ha CS. Preparation and characterization of polyimide/mesoporous silica hybrid nanocomposites based on water-soluble poly (amic acid) ammonium salt. Eur Polym J 2009;45: 19-29.

[11] Liu D, Geng L, Fu Y, Dai X, Lü C. Novel nanocomposite membranes based on sulfonated mesoporous silica nanoparticles modified sulfonated polyimides for direct methanol fuel cells. J Membrane Sci 2011;366: 251-257.

[12] Cheng CF, Cheng HH, Cheng PW, Lee YJ. Effect of reactive channel functional groups and nanoporosity of nanoscale mesoporous silica on properties of polyimide composite. Macromolecules 2006;39: 7583-7590.

[13] Min CK., Wu TB, Yang WT, Chen CL. Functionalized mesoporous silica/polyimide nanocomposite thin films with improved mechanical properties and low dielectric constant. Compos Sci Technol 2008;68: 1570-1578.

[14] Kapoor A, Bahadur S. Transfer film bonding and wear studies on CuS-nylon composite sliding against steel. Tribol Inter 1994;27: 323-329.

[15] Gao J. Tribochemical effects in formation of polymer transfer film. Wear 2000;245: 100-106.

[16] Li T, Cong P, Liu X, Tao J, Xue Q. Tribophysical and tribochemical effects of a thermoplastic polyimide. J Mater Sci 2000;35: 2597-2601.

[17] Samyn P, Schoukens G. The lubricity of graphite flake inclusions in sintered polyimides affected by chemical reactions at high temperatures. Carbon 2008;46: 1072-1084.

[18] Samyn P, De Baets P, Van Craenenbroeck J, Verpoort F, Schoukens G. Thermal transitions in polyimide transfer under sliding against steel, investigated by Raman spectroscopy and thermal analysis. J Appl Polym Sci 2006;101: 1407-1425.

[19] Samyn P, De Baets P, Vancraenenbroeck J, Verpoort F. Postmortem raman spectroscopy explaining friction and wear behavior of sintered polyimide at high temperature. J Mater Eng Perfor 2006;15: 750-757.

[20] Samyn P, Schoukens G. Thermochemical sliding interactions of short carbon fiber polyimide composites at high pv-conditions. Mater Chem Phys 2009;115: 185-195.

[21] Romanes MC, D'Souza NA, Coutinho D, Balkus KJ, Scharf TW. Surface and subsurface characterization of

epoxy-mesoporous silica composites to clarify tribological properties. Wear 2008;265: 88-96.
[22] Kosuge K, Singh PS. Mesoporous silica spheres via l-alkylamine templating route. Micropor Mesopor Mat 2001;44: 139-145.
[23] Rodriguez F, Cohen C, Ober C, Archer LA. In Principles of Polymer Systems. 5th ed. London: New York; 2003.
[24] Ji X, Hampsey JE, Hu Q, He J, Yang Z, Lu Y. Mesoporous silica-reinforced polymer nanocomposites. Chem Mater 2003;15: 3656-3662.
[25] Ver Meer MA, Narasimhan B, Shanks BH, Mallapragada SK. Effect of mesoporosity on thermal and mechanical properties of polystyrene/silica composites. ACS Appl Mater Inter 2009; 2: 41-47.
[26] Huang T, Xin Y, Li T, Nutt S, Su C, Chen H, Liu P, Lai Z. Modified graphene/polyimide nanocomposites: reinforcing and tribological effects. ACS Appl Mater Inter 2013;5: 4878-4891.
[27] Myshkin NK, Petrokovets MI, Kovalev AV. Tribology of polymers: Adhesion, friction, wear, and mass-transfer Tribol Int 2006;38: 910-921.
[28] Liu T, Rhee SK, Lawson KL. A study of wear rates and transfer films of friction materials. Wear 1980;60: 1-12.
[29] Ye J, Khare HS, Burris DL. Transfer film evolution and its role in promoting ultra-low wear of a PTFE nanocomposite. Wear 2013; 297: 1095-1102.
[30] Hatori H, Yamada Y, Shiraishi M, Yoshihara M, Kimura T. The mechanism of polyimide pyrolysis in the early stage. Carbon 1996; 34: 201-208.
[31] Bijwe J. Composites as friction materials: Recent developments in non−asbestos fiber reinforced friction materials-a review. Polym Composite1997; 18: 378-396.